Effect of uniaxial stress on the magnetic phases of CeAuSb_{2}

Joonbum Park, Hideaki Sakai, Andrew P. Mackenzie, and Clifford W. Hicks

Effect of uniaxial stress on the magnetic phases of CeAuSb$_2$

Joonbum Park,[1, 2, *] Hideaki Sakai,[3, 4] Andrew P. Mackenzie,[1, 5] and Clifford W. Hicks[1, †]

[1]*Max Planck Institute for Chemical Physics of Solids, Nöthnitzer Straße 40, 01187 Dresden, Germany*
[2]*Max Planck POSTECH Center for Complex Phase Materials,*
Pohang University of Science and Technology, Pohang 37673, Republic of Korea
[3]*Department of Physics, Osaka University, Toyonaka, Osaka 560-0043, Japan*
[4]*PRESTO, Japan Science and Technology Agency, Kawaguchi, Saitama 332-0012, Japan*
[5]*Scottish Universities Physics Alliance (SUPA), School of Physics and Astronomy,*
University of St. Andrews, St. Andrews KY16 9SS, United Kingdom
(Dated: July 5, 2018)

We present results of measurements of resistivity of CeAuSb$_2$ under the combination of c-axis magnetic field and in-plane uniaxial stress. In unstressed CeAuSb$_2$ there are two magnetic phases. The low-field A phase is a single-component spin density wave, with $\mathbf{q} = (\eta, \pm\eta, 1/2)$, and the high-field B phase consists of microscopically coexisting $(\eta, \eta, 1/2)$ and $(\eta, -\eta, 1/2)$ spin density waves. Pressure along a $\langle 100 \rangle$ lattice direction is a transverse field to both of these phases, and so initially has little effect, however eventually induces new low- and high-field phases in which the principal axes of the SDW components appear to have rotated to the $\langle 100 \rangle$ directions. Under this strong $\langle 100 \rangle$ compression, the field evolution of the resistivity is much smoother than at zero strain: In zero strain, there is a strong first-order transition, while under strong $\langle 100 \rangle$ it becomes much broader. We hypothesize that this is a consequence of the uniaxial stress lifting the degeneracy between the (100) and (010) directions.

INTRODUCTION

The magnetic order of CeAuSb$_2$ offers a compelling example of how electronic order can cause a reduction in the point-group symmetry of the host lattice. CeAuSb$_2$ is a layered, tetragonal compound in which a large-amplitude, incommensurate spin density wave condenses at $T_N = 6.5$ K (in zero applied field) [1]. It is a heavy-fermion system, with a Kondo temperature of ∼14 K [2]. The magnetic order shows entropy balance with a Fermi liquid, showing that at T_N the Ce spins are in fact incorporated into the Fermi sea through the Kondo effect [3]. For c-axis fields below ∼3 T, the in-plane wavevector of the SDW is, in reciprocal lattice units, either $(\eta, \eta, 1/2)$ or $(\eta, -\eta, 1/2)$, with $\eta \approx 0.136$ [1], and in selecting locally which of these two possibilities condenses, the point-group symmetry of the system is locally reduced from tetragonal to orthorhombic.

However CeAuSb$_2$ is highly polarizable under a c-axis magnetic field [4, 5], and as field is applied the modulation amplitude of the SDW decreases. At ∼3 T there is a first-order transition, above which the two components coexist microscopically. If their amplitudes are equal tetragonal symmetry is restored. The modulation persists up to ∼6 T, beyond which, at another first-order transition, the system becomes uniformly polarized [4, 6].

The association of weaker order with microscopic coexistence extends to other systems. The correlated-electron material Sr$_3$Ru$_2$O$_7$ has a magnetically ordered phase with low-amplitude SDWs oriented along the (100) and (010) directions, which coexist microscopically [7, 8]. In at least some iron-based superconductors, single-component C_2-symmetric magnetic order at low dopings gives way, as the order is suppressed through doping towards its quantum critical point, to two-component C_4-symmetric order [9, 10]. In the rare-earth tritelluride compounds, which are weakly orthorhombic, charge density waves with perpendicular wavevectors can coexist microscopically, however only when the amplitude of the dominant component is suppressed through chemical pressure [11, 12]. An advantage of studying CeAuSb$_2$ is that the strength of the density wave order, and, apparently, the strength of competition between the two possible density wave components, can be tuned externally with magnetic field.

The transition at ∼3 T in CeAuSb$_2$ is a single- to multi-component transition, and probably also an orthorhombic to tetragonal transition. The above-listed systems may have similar transitions, driven by a tuning parameter such as doping or magnetic field. We hypothesize that the single- to multi-component transition in CeAuSb$_2$ is first-order because there is no natural pathway to tune between the two phases, and further that an externally-applied symmetry-breaking field such as in-plane uniaxial stress could provide such a pathway and change the transition into a continuous (*i.e.* second-order) transition. Under tetragonal lattice symmetry the two components are degenerate, and the two natural possibilities for T well below T_N are that strong competition allows only one component to condense, yielding spontaneous symmetry breaking, or that weaker competition allows them to coexist microscopically with equal amplitude. A transition between these states would be strongly discontinuous. However in-plane uniaxial stress would lift the degeneracy and may allow one component to dominate on both sides of a single- to multi-component transition, and the amplitude of the other to grow con-

tinuously from zero.

Here, we test this hypothesis in two stages. First, we test whether the high-field phase (between ~ 3 and ~ 6 T) is in fact tetragonal. In principle, it is possible to have states with, in the absence of any symmetry-breaking field, $|\Delta_{11}| \neq |\Delta_{1\bar{1}}|$ and both $|\Delta_{11}|$ and $|\Delta_{1\bar{1}}| \neq 0$ [where Δ_{11} and $\Delta_{1\bar{1}}$ are respectively the the amplitudes of the $(\eta, \eta, 1/2)$ and $(\eta, -\eta, 1/2)$ density waves]. However this would require a more delicate tuning of interactions— more precisely, terms beyond fourth order in a two-component Ginzburg-Landau theory. We test for such symmetry breaking by ramping the applied uniaxial stress through zero (that is, between compressive and tensile). If there is spontaneous symmetry breaking, there should be a first-order transition at zero stress, where the favored direction of the symmetry breaking flips. In our earlier study of CeAuSb$_2$ under uniaxial stress and at zero field (Ref. [13]), such a transition was observed, corresponding to the transition between $\mathbf{q} = (\eta, \eta, 1/2)$ and $(\eta, -\eta, 1/2)$. However, here, to high sensitivity no such transition is observed for the high-field phase, indicating that it is most likely tetragonal (*i.e.* $|\Delta_{11}| = |\Delta_{1\bar{1}}|$).

Second, we apply strong uniaxial compression and observe the evolution of the field-temperature phase diagram. We focus mostly on stress along $\langle 100 \rangle$ directions (that is, Ce-Ce bond directions). Although the density wave components in unstressed CeAuSb$_2$ are oriented along $\langle 110 \rangle$ directions and $\langle 100 \rangle$ stress is a transverse field to this order, stress along $\langle 110 \rangle$ directions has a much smaller quantitative effect than $\langle 100 \rangle$ stress [13]. Here, at the strongest applied $\langle 110 \rangle$ compression the transition at ~ 3 T broadens only slightly, and it is difficult to be confident that this observed change is intrinsic. In the previous study it was found that $\langle 100 \rangle$ compression by $\sim 0.5\%$ almost certainly rotates the principal axes of the low-field magnetic order from $\langle 110 \rangle$ to $\langle 100 \rangle$. Therefore, we work primarily with $\langle 100 \rangle$ stress, and compressions of $\sim 0.5\%$ and higher.

SUMMARY OF PREVIOUS RESULTS

We begin by providing more detail, in Fig. 1, on previous results. The field-temperature phase diagram of unstressed CeAuSb$_2$ is shown in panel (a) [3, 4]. The metamagnetic transitions occur at $\mu_0 H_1 = 2.8$ T and $\mu_0 H_2 = 5.9$ T. We label the low- and high-field phases the A and B phases.

The magnetic order of CeAuSb$_2$ has been shown to be sensitive to hydrostatic pressure, with a modest pressure of ~ 2 GPa inducing a new magnetic phase [2]. It is similarly sensitive to uniaxial stress applied along a $\langle 100 \rangle$, but not a $\langle 110 \rangle$, direction. In panel (b) we show the stress-temperature phase diagram at zero field for stress applied along a $\langle 110 \rangle$ direction, inducing a longitudinal
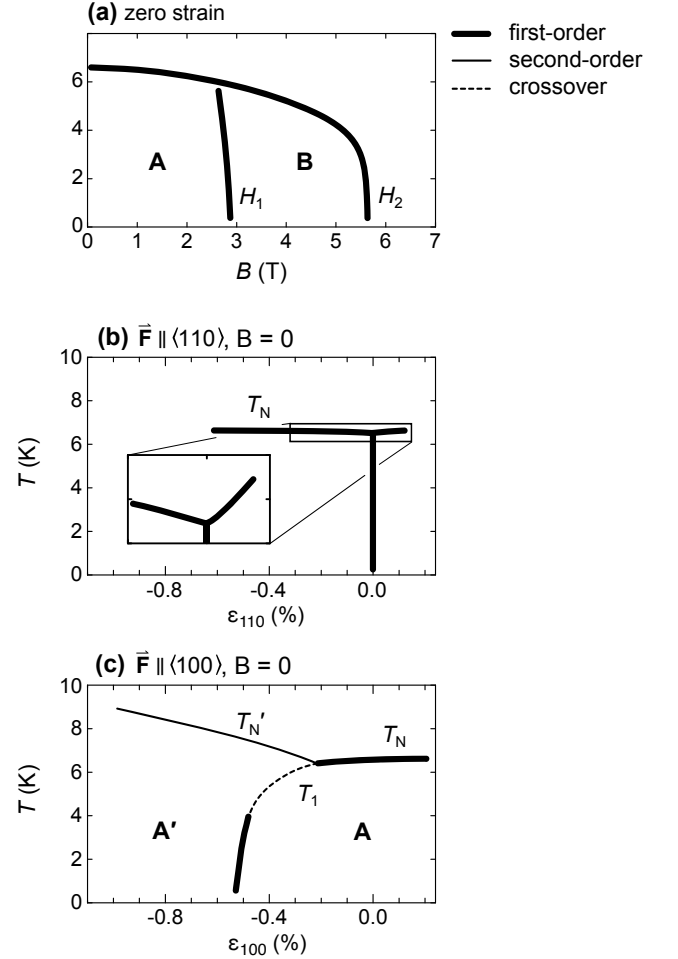

FIG. 1: (a) Field-temperature phase diagram of unstressed CeAuSb$_2$, for field along the c axis. In Ref. [3] the near-vertical transition lines at H_1 and H_2 were found to be first-order, and in Ref. [13] the transition at $H = 0$, $T = T_N$ was also found to be, probably, weakly first-order. (b) and (c) Schematic $H = 0$ strain-temperature phase diagrams, such as they could be resolved in measurements, in panel (b) for pressure applied along a $\langle 110 \rangle$ lattice direction, and in panel (c) a $\langle 100 \rangle$ direction.

strain ε_{110} [13]. (The sample is under conditions of uniaxial stress, so there will also be transverse strains of the opposite sign, following the sample's own Poisson's ratios) The line of first-order transitions along $\varepsilon_{110} = 0$ shows that the magnetic order spontaneously lifts the $(110)/(1\bar{1}0)$ symmetry of the $T > T_N$ lattice. However, despite this notable qualitative effect, the quantitative effect of $\langle 110 \rangle$ stress on T_N is small.

In panel (c) we show the stress-temperature phase diagram for $\langle 100 \rangle$ stress. When CeAuSb$_2$ is compressed by more than $\sim 0.25\%$ along a $\langle 100 \rangle$ direction, the transition at T_N splits into two transitions, at temperatures T_1 and T'_N. The transition at T'_N is second-order. $T_1 \to 0$ at a compression of about 0.5%, and we label the new high-strain phase A'. $\langle 100 \rangle$ strain is a transverse field with

respect to the A phase, which has $\langle 110 \rangle$ principal axes, so it is not surprising that T_N varies only weakly with ε_{100}. The much stronger, linear dependence of T_N' on ε_{100} is strong evidence that $\langle 100 \rangle$ strain is a longitudinal field with respect to the A$'$ phase, in other words that the principal axes have rotated to the $\langle 100 \rangle$ directions. This would occur if, for example, the in-plane SDW wavevector rotated from $(\eta, \pm\eta)$ to $(\eta', 0)$ or $(0, \eta')$.

The transition between the A and A$'$ phases is first-order below ≈ 4 K, and in resistivity data appears to be a crossover above. However if different symmetries are broken in the A and A$'$ phases there must be a true transition line between them.

METHODS

CeAuSb$_2$ crystals were grown according to the methods described elsewhere [14, 15]. They were oriented to a precision of $\sim 3°$ by Laue diffraction, then beams were cut from the crystals with the long axis along a $\langle 100 \rangle$ or $\langle 110 \rangle$ direction. The crystals naturally grow in a plate-like geometry, however they were further polished in order to obtain a uniform sample thickness. The samples were then mounted into home-built uniaxial pressure apparatus [16] (using Stycast 2850FT epoxy), in which force is applied along their long axis. The pressure apparatus is driven by piezoelectric actuators. It incorporates a displacement sensor placed in parallel with the sample. As in previous reports [8, 13], we estimate that $\sim 80\%$ of the applied displacement is transferred to the central, exposed portion of the sample, with the rest going into deformation of the ends of the sample and the epoxy. In other words, the strains reported here are the applied displacement divided by the exposed length of the sample, multiplied by 0.8, and we estimate a $\sim 20\%$ sample-to-sample error on this strain determination.

We measured a total of six samples, two cut along a $\langle 110 \rangle$ direction and four along a $\langle 100 \rangle$ direction. The first five samples were also studied in Ref. [13], and have the same numbering here.

For the $\langle 110 \rangle$ samples, zero strain was taken as the location of the first-order transition: This transition is expected to occur at zero strain, there is no other feature that could mark the neutral strain point, and, finally, taking it to mark zero implies a room temperature to 0 K thermal contraction for CeAuSb$_2$ of $\sim 0.25\%$, which is a typical value for a metal. For the $\langle 100 \rangle$ samples, there is no feature in the response at the neutral strain point, so we took zero strain to be at the same applied displacement as for the $\langle 110 \rangle$ samples.

The resistivity of CeAuSb$_2$ changes strongly at the Néel transition and also across the metamagnetic transitions. In principle, when measuring resistivity under uniaxial stress the results should be corrected for a geometric contribution, which is the change in resistance that would still be observed if the sample resistivity were held constant, due to the applied change in sample dimensions. However, the resistivity of CeAuSb$_2$ varies strongly with strain and we neglect this correction.

RESULTS: TESTING THE SYMMETRY OF THE HIGH-FIELD PHASE

Fig. 2 shows the results of ramping the stress applied along a $\langle 110 \rangle$ direction, at various fixed fields H and $T = 1.7$ K. Below H_1 (the transition field between the A and B phases), the resistivity shows a step-like response across $\varepsilon_{110} = 0$. There is clear hysteresis between the increasing- and decreasing-strain ramps. This is the first-order transition between $(\eta, \eta, 1/2)$ and $(\eta, -\eta, 1/2)$ spin density wave order, and the presence of this transition proves that the A phase is C_2-symmetric. The hysteresis shrinks as the field is increased, implying a decreasing energy barrier for flipping domains.

At fields around H_1 and H_2, there are first-order transitions at $\varepsilon_{110} \neq 0$, which correspond respectively to strain-driven transitions between the A and B phases, and between the B phase and high-field paramagnetic phase. However, as shown in the inset of Fig. 2(a), to high precision there is no first-order transition across $\varepsilon_{110} = 0$ within the B phase. We conclude that it most likely preserves symmetry between the (110) and $(1\bar{1}0)$ directions.

Equivalent data for stress ramps along a $\langle 100 \rangle$ direction are shown in Fig. 3, with the temperature held constant at 1.5 K. For fields below 3 T, the transition between the A and A$'$ phases is visible as a sharp change in slope of $\rho(\varepsilon_{100})$, at $\varepsilon_{100} \sim -0.5\%$. The hysteresis that shows that this transition is first-order is not visible in the figure, however was resolved in Ref. [13]. There also appears to be a similar transition at high compressions: for $|\varepsilon_{100}| < \sim 0.5\%$, ρ is nearly strain-independent, then at higher compressions there is a transition into a state with much greater sensitivity to ε_{100}. We will discuss this further later. Finally, for fields right in the vicinity of H_1, the resistivity is strongly hysteretic.

For our present purpose, the important feature in Fig. 3 is that there is no apparent transition at $\varepsilon_{100} = 0$, either in the low-field or high-field phase. Our sensitivity to changes in ρ was $\delta\rho/\rho \sim 10^{-4}$. We conclude that the magnetic order in both phases most likely preserves the symmetry between the (100) and (010) directions. Because the data in Fig. 2 indicate that the B phase also preserves $(110)/(1\bar{1}0)$ symmetry, we conclude that it is probably C_4-symmetric, $i.e.$ tetragonal.

In Ref. [1], it was proposed that the B phase may possess a subtle symmetry-breaking between the (100) and (010) lattice directions. The neutron data are consistent both with a multi-component checkerboard order, which preserves $(100)/(010)$ symmetry, and a "woven" order,
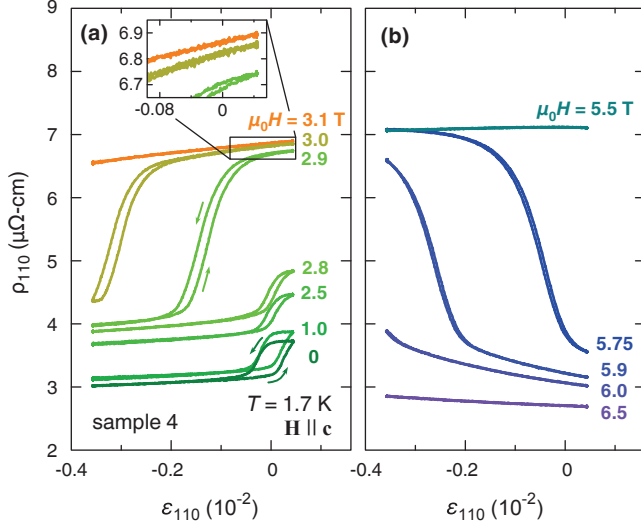
FIG. 2: (color online) $\rho_{110}(\varepsilon_{110})$ **at selected magnetic fields.** ρ_{110} is the resistivity measured along the length of the sample, cut along a $\langle 110 \rangle$ direction, and ε_{110} the longitudinal strain achieved through uniaxial stress applied along this sample. (a) The data taken between $H = 0$ and $H = 3.1$ T, and (b) between $H = 5.5$ T and $H = 6.5$ T.

FIG. 3: (color online) $\rho_{100}(\varepsilon_{100})$ **at selected magnetic fields.** ρ_{100} is the resistivity measured along the length of the sample, cut along a $\langle 100 \rangle$ direction, and ε_{100} the longitudinal strain achieved through uniaxial stress applied along this sample. (a) The data taken between $H = 0$ and $H = 5.0$ T, and (b) between $H = 5.5$ T and $H = 6.5$ T.

which like the checkerboard order is a multi-component density wave, but in which the local pattern of magnetization lifts $(100)/(010)$ symmetry. It was speculated that the woven order might be favored because it allows each component to have a larger amplitude while keeping the local maximum and minimum magnetizations within a narrower range. In principle, because the symmetry breaking in the proposed woven order is subtle, its effect on resistivity could yet be below our resolution. However we conclude that it is more likely that the B phase is in fact the tetragonal, checkerboard order.

RESULTS: LARGE STRAINS

We start, in Fig. 4, with the results from large $\langle 110 \rangle$ strain, which essentially confirm the finding of Ref. [13] that the quantitative coupling of $\langle 110 \rangle$ orthorhombicity to the magnetic order is weak. The figure shows results of measurement of $\rho(H)$ at various fixed strains ε_{110}, and $T = 1.7$ K. The form of $\rho_{110}(H)$, a first-order increase at H_1 and first-order decrease at H_2, is familiar from previous studies [3, 4, 6]. Field sweeps reported in previous studies confirmed that these are first-order transitions, with hysteresis. Both transitions move to modestly higher fields with $\langle 110 \rangle$ compression. The transition at H_1 broadens slightly as the sample is compressed, and arguably, looking at the highest compression, slightly more than the transition at H_2. This broadening could be an early sign of the hypothesized stress-driven evolution from a first-order to a continuous transition. However it
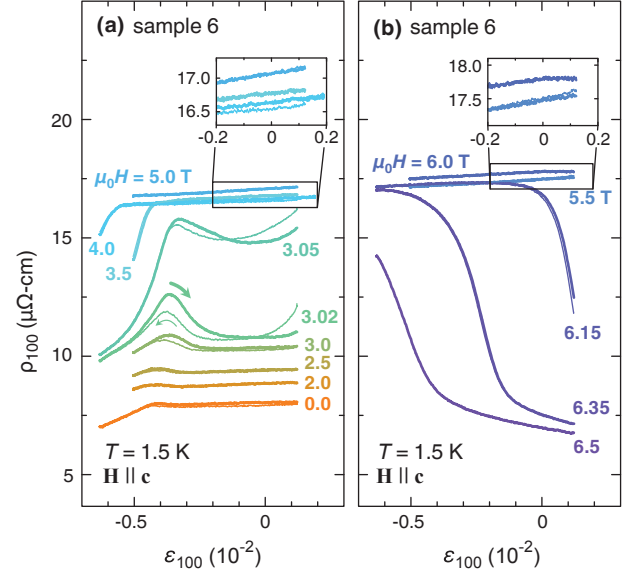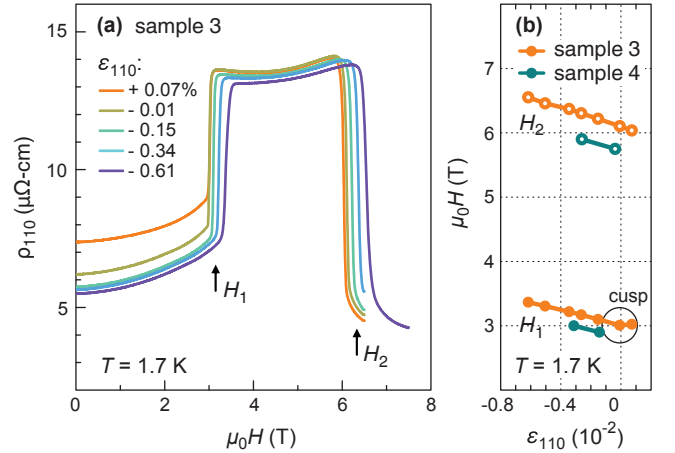

FIG. 4: (color online) (a) $\rho_{110}(H)$ at selected $\langle 110 \rangle$ strains, where the temperature was kept constant at $T = 1.7$ K. (b) The $H - \varepsilon_{110}$ phase diagram for $T = 1.7$ K. Here, the H_1 and H_2 data points for sample 3 were taken from the field derivative maxima and the minima, whereas for sample 4, points were taken from the mid-point of the step-like transition.

could also be an extrinsic effect of stress gradients in the sample, due to minor bending of the sample as stress is applied.

As highlighted in Fig. 4(b), $H_1(\varepsilon_{110})$ shows a cusp at zero strain, consistent with the above-described observations that the A phase lifts the $(110)/(1\bar{1}0)$ symmetry of the lattice. No such cusp is apparent in H_2, consis-

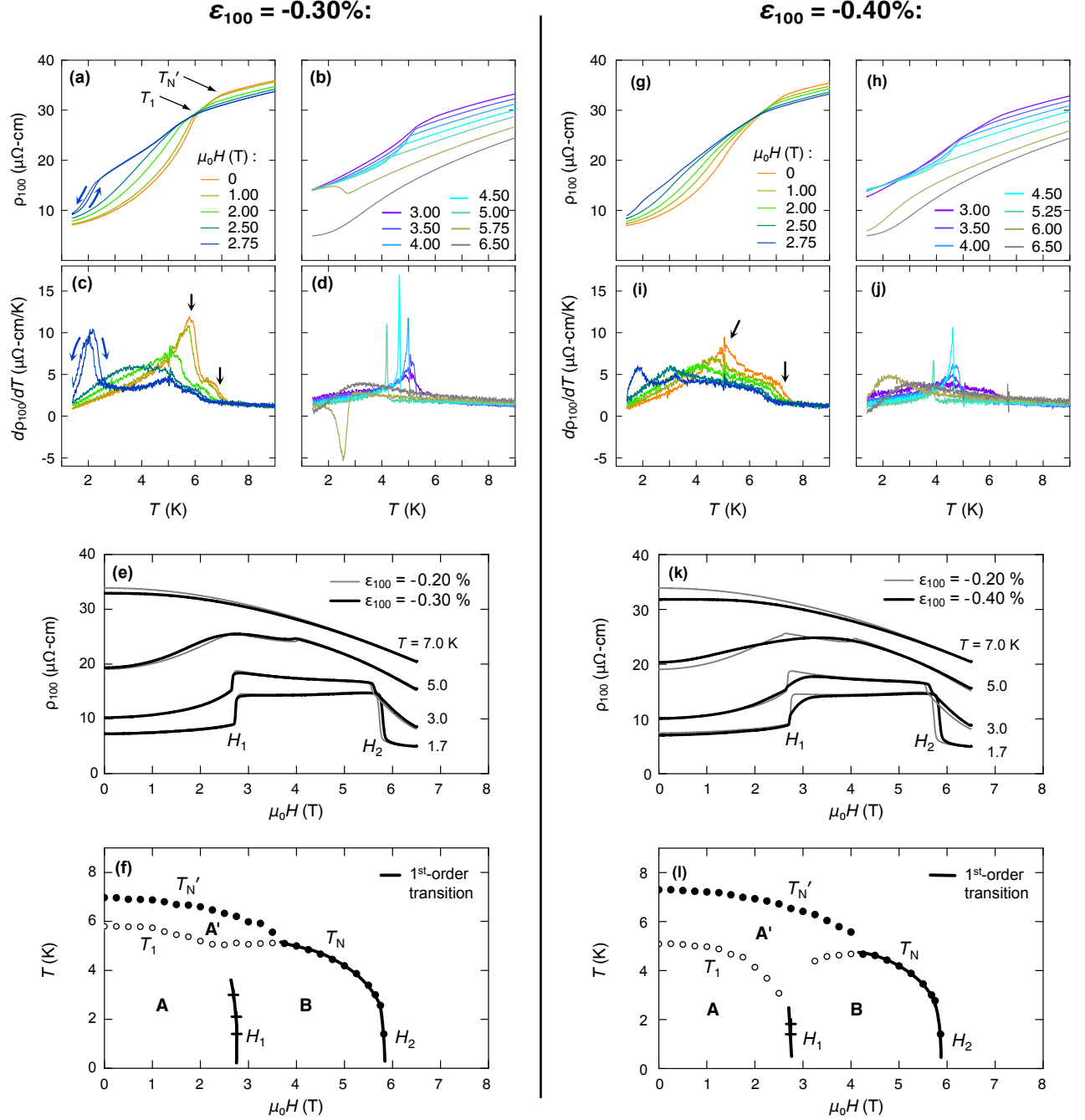**ε₁₀₀ = -0.30%:**

ε₁₀₀ = -0.40%:

FIG. 5: (color online) Field-temperature phase diagrams under applied compression along a $\langle 100 \rangle$ direction. Data are from sample 2. **(a-f) 0.3% compression.** (a) and (b): $\rho_{100}(T)$ at selected magnetic fields for (a) $H < H_1$ and (b) $H > H_1$. (c) and (d): Derivatives $d\rho_{100}/dT$ of the curves in, respectively, panels (a) and (b). (e) $\rho_{100}(H)$ at selected fixed temperatures, plotted together with, for reference, data at $\varepsilon_{100} = -0.2$ %. (f) The field-temperature phase diagram derived from the data in panels (a-e). **(g-l) 0.4% compression.** The panels mirror panels (a-f).

tent with our finding above that the high-field phase is probably C_4-symmetric.

We move on to large $\langle 100 \rangle$ stress, for which the response is considerably richer. To understand the evolution of the field-temperature phase diagram, we start in Fig. 5 with relatively low strains, $\varepsilon_{100} = -0.3$ and -0.4%,

where there are observable changes in the phase diagram, but where the connections with the zero-strain phase diagram also remain clear. Results for $\varepsilon_{100} = -0.3\%$ are shown in panels (a)-(f), and show that at this strain the field-temperature phase diagram is only minimally altered from that at zero strain. As was reported in

Ref. [13], this is a large enough strain to split the Néel transition (into the transitions at temperatures T_1 and T_N'). This splitting is observable as two breaks in slope in the $\rho(T)$ curves shown in panel (a), and can also be seen as two step-like features in the derivative $d\rho/dT$, shown in panel (c). The splitting persists, essentially unchanged, for all fields $H < H_1$.

At 2.75 T, right in the vicinity of $\mu_0 H_1$, a very prominent first-order transition appears at ~ 2 K. This is the transition between the A and B phases, visible in a temperature ramp because the transition line is not perfectly vertical in field-temperature space.

Separate transitions at T_1 and T_N' remain visible at H_1. As H is further increased [see panels (b) and (d), which show the data for $H > H_1$], the splitting decreases and the transitions merge at $\mu_0 H \approx 3.6$ T. At higher fields the transition into the B phase occurs, as at zero strain, through a single, first-order transition. The first-order nature of the transition is apparent in the very sharp peaks in $d\rho_{100}/dT$, in panel (d).

To identify any changes in $H_1(T)$ and $H_2(T)$, field ramps were performed at constant temperature, with the results shown in panel (e). They are shown together with data from field ramps at $\varepsilon_{100} = -0.2\%$, which match the zero-strain data very well [3]. The increase in strain from -0.2 to -0.3% induces very little change; the only substantial qualitative change is that at $T = 5$ K there is no longer an identifiable transition at H_1.

Putting all this data together, we obtain a field-temperature phase diagram for $\varepsilon_{100} = -0.3\%$, shown in panel (f). It is qualitatively similar to the field-temperature phase diagram of the unstressed sample, except in a narrow band along the $T_N(H)$ line where the A$'$ phase has appeared.

In panels (g)-(l) we show the equivalent data for a higher strain, $\varepsilon_{100} = -0.4\%$. The data are qualitatively similar to those at $\varepsilon_{100} = -0.3\%$, though show stronger effects from the applied lattice orthorhombicity. Most obviously, the A$'$ phase now occupies a larger region of the phase diagram. Another prominent change is that the first-order transition between the A and B phases has become considerably weaker. In panel (e), where $\varepsilon_{100} = -0.3\%$, the first-order step in ρ constitutes almost the entire transition, while in panel (k), where $\varepsilon_{100} = -0.4\%$, the first-order step is only a small feature in a transition that overall has become broad and rounded.

Fig. 6 presents data at stronger compressions. $\rho(H)$ is shown for various fixed strains ε_{100} in panel (a). As the A phase is fully suppressed and replaced even at $T \to 0$ by the A$'$ phase, the transition at H_1 disappears completely. A new first-order transition appears, at a field that we label H_1'. The similarity of H_1 and H_1' indicate that the physical process driving these transitions is likely to be similar; we hypothesize that both are single-to multi-component transitions. However the form of the
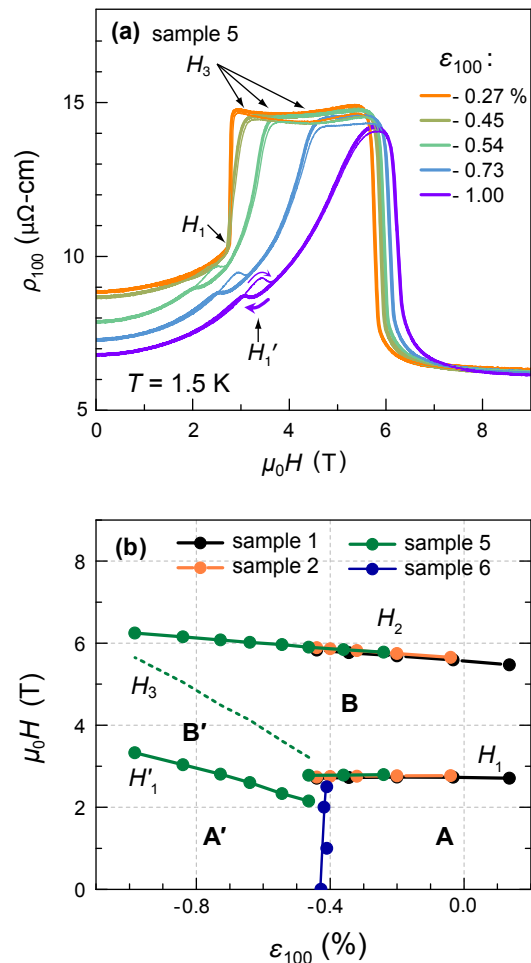

FIG. 6: (a) $\rho_{100}(H)$ at selected fixed strains ε_{100} and $T = 1.5$ K. (b) $H - \varepsilon_{100}$ phase diagram at $T = 1.5$ K.

transition at H_1' is different from that at H_1: the hysteresis is much wider, and the change in ρ across the transition is much smaller. It is also apparent in Fig. 6(a) that whereas H_1 is nearly independent of ε_{100}, H_1' varies rapidly with ε_{100}. The strain dependence of H_1 and H_1' can also be seen in the strain-temperature phase diagram for $T = 1.5$ K, shown in panel (b). It is a similar situation to T_N and T_N', where the former is nearly invariant with ε_{100} while the latter has a strong linear dependence, and constitutes further evidence that the principal axes have rotated to the $\langle 100 \rangle$ directions in the A$'$ phase.

Two further features apparent in Fig. 6(a) should be noted. One is that the resistivity varies much more strongly with ε_{100} in the A$'$ than the A phase: $\rho(H)$ for $H < H_1$ changes very little with ε_{100} for $|\varepsilon_{100}| < 0.5\%$, but varies much more rapidly at larger compressions. Another is that a set of transition fields that we label H_3 have appeared in the high-field phase. Below H_3, ρ varies strongly with both field and ε_{100}, while above it is nearly strain- and field-independent. In the phase diagram of

Fig. 6(b), we identify H_3 as a transition line into a high-strain, high-field phase that we label B′. This transition is also visible in the $\rho(\varepsilon_{100})$ data shown in Fig. 3(a). As a summary of our data, we present in Fig. 7 a three-dimensional field-strain-temperature phase diagram.

DISCUSSION

We have presented evidence that the B phase, in contrast to the A phase, does not lift the C_4 symmetry of the lattice of CeAuSb$_2$. We have also shown that the field-temperature phase diagram of CeAuSb$_2$ has a rich dependence on applied $\langle 100 \rangle$ orthorhombicity. At a minimum, we have identified the strains and fields where transitions in the magnetic order occur. Definitive identification of how the magnetic order changes under strain will require further measurements, for example neutron scattering on uniaxially stressed CeAuSb$_2$. We proceed in our discussion with inferences that might be drawn based on the resistivity alone.

The H-ε_{100} phase diagram of Fig. 6(b) is essentially a 2×2 grid, where the small-$|\varepsilon_{100}|$ phases are A and B, and the large-$|\varepsilon_{100}|$ phases A′ and B′. Neutron scattering data [1] have shown that the A and B phases are respectively single- and multi-component orders. From the quantitative similarity of H_1 and H_1', the transition field between the A′ and B′ phases, we hypothesize that the A′ and B′ phases are also, respectively, single- and multi-component orders.

Both the A′ and B′ phases are marked by a much stronger sensitivity to applied $\langle 100 \rangle$ lattice orthorhombicity than the A and B phases. The resistivity varies much more strongly with ε_{100} in both the A′ and B′ phases than in the A and B phases, and the transition fields that bound the A′ and B′ phases, H_1' and H_3, vary more rapidly with ε_{100} than those bounding the A and B phases, H_1 and H_2. We therefore conclude that $\langle 100 \rangle$ orthorhombicity is a longitudinal field for both the A′ and B′ phases, where it is a transverse field for the A and B phases; in other words the density wave components comprising both the A′ and B′ phases have $\langle 100 \rangle$ principal axes. The 2×2 grid therefore appears to comprise the possible combinations of single- and multi-component order, and $\langle 110 \rangle$ and $\langle 100 \rangle$ principal axes.

It is interesting that the B phase is, apparently, so insensitive to ε_{100}. In the neutron study [1], strong scattering peaks were observed at wavevectors $(2\eta, 0, 0)$ and $(0, 2\eta, 0)$, which were interpreted as results of nonlinear mixing of the $(\eta, \pm\eta, 1/2)$ components. If we interpret the ε_{100}-independence of ρ within the B phase as indicating that the magnetic order is similarly unaffected by ε_{100}, then our observations support this interpretation. The magnetic order, until the boundary with the B′ phase is reached, is essentially independent of ε_{100} because $\langle 100 \rangle$ orthorhombicity is a transverse field to the
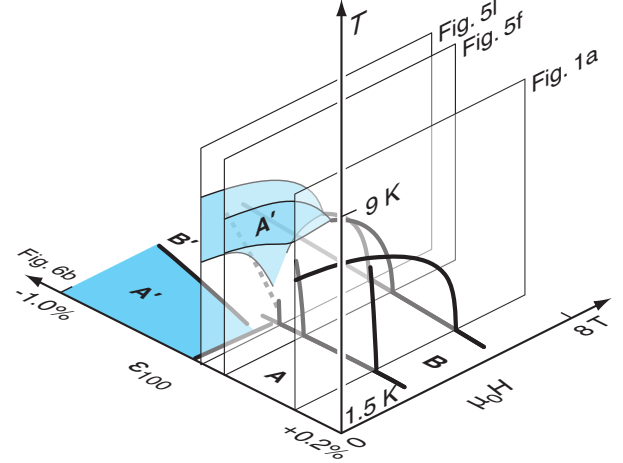

FIG. 7: The field-strain-temperature phase diagram of CeAuSb$_2$ under applied $\langle 100 \rangle$ uniaxial pressure.

two fundamental components, and the peaks at $(2\eta, 0, 0)$ and $(0, 2\eta, 0)$ are interference peaks, not independent components that couple directly to $\langle 100 \rangle$ orthorhombicity.

We conclude by returning to our original hypothesis that applied lattice orthorhombicity, by selecting a preferred direction, would change the first-order transition at H_1 into a continuous transition. The high-strain data partially but not completely support this hypothesis. Instead of a dominant first-order step at H_1, under large $|\varepsilon_{100}|$ the field evolution of the resistivity, and by inference the magnetic order, is overall more gradual. However there is still a first-order transition, at H_1'. The change in ρ across H_1' is small, suggesting that the change in magnetic order is minimal. It is possible that higher-order interactions still drive the single- to multi-component transition first-order, and the weaker component onsets with small but non-infinitesimal amplitude.

for Young Scientists (No. 16H06015). Raw data for all figures in this paper are available at *to be determined*.

————————

* Electronic address: jbpark0521@gmail.com

† Electronic address: hicks@cpfs.mpg.de

[1] G. G. Marcus, D.-J. Kim, J. A. Tutmaher, J. A. Rodriguez-Rivera, J. O. Birk, C. Niedermeyer, H. Lee, Z. Fisk, and C. L. Broholm, Multi-q Mesoscale Magnetism in CeAuSb$_2$. *Phys. Rev. Lett.* **120**, 097201 (2018).

[2] S. Seo, V. A. Sidorov, H. Lee, D. Jang, Z. Fisk, J. D. Thompson, and T. Park, Pressure effects on the heavy-fermion antiferromagnet CeAuSb$_2$. *Phys. Rev. B* **85**, 205145 (2012).

[3] L. Zhao, E. A. Yelland, J. A. N. Bruin, I. Sheikin, P. C. Canfield, V. Fritsch, H. Sakai, A. P. Mackenzie, and C. W. Hicks, Field-temperature phase diagram and entropy landscape of CeAuSb$_2$. *Phys. Rev. B* **93**, 195124 (2016).

[4] L. Balicas, S. Nakatsuji, H. Lee, P. Schlottmann, T. P. Murphy, and Z. Fisk, Magnetic field-tuned quantum critical point in CeAuSb$_2$. *Phys. Rev. B* **72**, 064422 (2005).

[5] A. Thamizhavel, T. Takeuchi, T. Okubo, M. Yamada, R. Asa, S. Kirita, A. Galatanu, E. Yamamoto, T. Ebihara, Y. Inada, R. Settai, and Y. Ōnuki, Anisotropic electrical and magnetic properties of CeTSb$_2$ (T = Cu, Au, and Ni) single crystals. *Phys. Rev. B* **68**, 054427 (2003).

[6] K.-A. Lorenzer, A. M. Strydom, A. Thamizhavel, and S. Paschen. Temperaturefield phase diagram of quantum critical CeAuSb$_2$. *Phys. Status Solidi B* **250**, 464 (2013).

[7] C. Lester, S. Ramos, R. S. Perry, T. P. Croft, R. I. Bewley, T. Guidi, P. Manuel, D. D. Khalyavin, E. M. Forgan, and S. M. Hayden, Field-tunable spin-density-wave phases in Sr$_3$Ru$_2$O$_7$. *Nat. Materials* **14**, 373 (2015).

[8] D. O. Brodsky, M. E. Barber, J. A. N. Bruin, R. A. Borzi, S. A. Grigera, R. S. Perry, A. P. Mackenzie, and C. W. Hicks, Strain and vector magnetic field tuning of the anomalous phase in Sr$_3$Ru$_2$O$_7$. *Science Advances* **3**, 2, e1501804 (2017).

[9] S. Avci *et al*, Magnetically driven suppression of nematic order in an iron-based superconductor. *Nat. Communications* **5** 3845 (2014).

[10] A. E. Böhmer, F. Hardy, L. Wang, T. Wolf, P. Schweiss, and C. Meingast, Superconductivity-induced re-entrance of the orthorhombic distortion in Ba$_{1-x}$K$_x$Fe$_2$As$_2$. *Nat. Communications* **6** 7911 (2015).

[11] N. Ru, C. L. Condron, G. Y. Margulis, K. Y. Shin, J. Laverock, S. B. Dugdale, M. F. Toney, and I. R. Fisher, Effect of chemical pressure on the charge density wave transition in rare-earth tritellurides RTe$_3$. *Phys. Rev. B* **77**, 035114 (2008).

[12] R. G. Moore, V. Brouet, R. He, D. H. Lu, N. Ru, J.-H. Chu, I. R. Fisher, and Z.-X. Shen, Fermi surface evolution across multiple charge density wave transitions in ErTe$_3$. *Phys. Rev. B* **81**, 073102 (2010).

[13] J. Park, H. Sakai, O. Erten, A.P. Mackenzie, and C.W. Hicks, Effect of applied orthorhombic lattice distortion on the antiferromagnetic phase of CeAuSb$_2$. *Phys. Rev. B* **97**, 024411 (2018).

[14] P. C. Canfield and Z. Fisk, *Philos. Mag. B* **65**, 1117 (1992).

[15] P. C. Canfield and I. R. Fisher, *J. Cryst. Growth* **225**, 155 (2001).

[16] C. W. Hicks, M. E. Barber, S. D. Edkins, D. O. Brodsky and A. P. Mackenzie, Piezoelectric-based apparatus for strain tuning. *Rev. Sci. Instrum.* **85**, 065003 (2014).